Microsaccades are triggered by low retinal image slip

Ralf Engbert* and Konstantin Mergenthaler

Department of Psychology and Helmholtz Center for Mind and Brain Dynamics, University of Potsdam, P.O. Box 60 15 53, 14415 Potsdam, Germany

Edited by Dale Purves, Duke University Medical Center, Durham, NC, and approved March 14, 2006 (received for review November 3, 2005)

Even during visual fixation of a stationary target, our eyes perform rather erratic miniature movements, which represent a random walk. These ''fixational'' eye movements counteract perceptual fading, a consequence of fast adaptation of the retinal receptor systems to constant input. The most important contribution to fixational eye movements is produced by microsaccades; however, a specific function of microsaccades only recently has been found. Here we show that the occurrence of microsaccades is correlated with low retinal image slip ≈200 ms before microsaccade onset. This result suggests that microsaccades are triggered dynamically, in contrast to the current view that microsaccades are randomly distributed in time characterized by their rate-of-occurrence of 1 to 2 per second. As a result of the dynamic triggering mechanism, individual microsaccade rate can be predicted by the fractal dimension of trajectories. Finally, we propose a minimal computational model for the dynamic triggering of microsaccades.

random walks | visual fixation | eye movements | saccade detection

The human visual system rapidly adapts to stationary input, which causes perceptual fading when the retinal image is stabilized artificially in the experimental paradigm of retinal stabilization (1, 2). Equipped with such a visual system optimized for the detection of approaching predators or escaping prey, we are unable to process fine details of completely stationary objects. As a consequence, our eyes must produce miniature (or ''fixational'') eye movements to counteract perceptual fading by actively refreshing retinal input for the optimal perception of stationary objects (3, 4). Among the three distinct types of fixational eye movements (drift, tremor, and microsaccades), microsaccades represent the fastest component with the largest amplitude (5–7) and occur at an average rate of 1 to 2 per second. The trajectory generated by fixational eye movements is rather erratic and has statistical properties of a random walk (8–10). Embedded in slower movements (drift and tremor), microsaccades are ballistic jumps (<1°) of the eye (Fig. 1 *Upper Left*), which represent roughly linear movement epoches. Here we investigate the generating process for microsaccades, in particular, we are interested in the question whether the temporal statistics of microsaccades represent a simple random process, i.e., a Poisson process (11), or whether microsaccades are triggered dynamically on demand by perceptual needs.

To find a specific role for microsaccades is a long-standing research problem (7, 12). First, an early hypothesis was that the function of microsaccades is to correct displacements in eye position produced by drifts (1, 6, 13, 14). According to this view, the probability of occurrence, direction, and amplitude of microsaccades must be correlated with the displacement generated by drift. No reliable correlation has been found, however, because microsaccades can be error-correcting and, at times, error-producing (8, 13). One solution to this problem might be related to a time-scale separation in microsaccade dynamics: On a short time scale, microsaccades are mainly error-producing (i.e., microsaccade enhance retinal image slip), whereas on a long time scale, microsaccades correct errors and help to maintain the current fixation position (8). Second, during high-acuity observational tasks like threading a needle, participants naturally suppressed microsaccades without training (15, 16). Moreover, trained participants were able to suppress their microsaccades for several seconds without fading of the image (17). As a consequence of these findings, in 1980, Kowler and Steinman (18) concluded that ''microsaccades serve no useful purpose'' and represent an ''evolutionary puzzle.''

Recently, it was demonstrated that microsaccades enhance the visibility of a peripheral stimulus (19) by using the paradigm of Troxler fading. This important finding represents a direct link between microsaccade activity and visual perception. Having identified such a function for perception, microsaccades still might be generated by a random process; however, a dynamical triggering mechanism is a potential alternative as a generating process. We carried out two experiments to investigate these alternative hypotheses.

Results

Given the basic function of fixational eye movements to counteract retinal fatigue by producing retinal image slip, we investigated whether microsaccades are triggered dynamically, whenever slow movements (drift and tremor) might be ineffective to generate sufficient retinal image slip. In two experiments, we monitored fixational eye movements during a simple fixation task. Human participants were asked to fixate a small dot on a computer display (see *Methods*). In experiment (Exp.) 1, participants performed 100 trials with a duration of 3 s; in Exp. 2, participants performed 30 trials with a duration of 20 s.

Detection of Microsaccades. Microsaccades were detected by using an improved version of a velocity-based algorithm proposed earlier (20). The time series of fixation positions was transformed into 2D velocity space (Fig. 1 *Upper Right*). Separate thresholds were computed for horizontal and vertical velocities, constituting an elliptic threshold in 2D velocity space. Thresholds were relative to the noise level, calculated as $\lambda = 5$ multiples of a median-based SD estimator. Because microsaccades are ballistic movements with the same kinematic properties as normal saccades (21), there is a high correlation ($r = 0.92$; $P < 10^{-6}$) between microsaccade amplitude and peak velocity (Fig. 1 *Lower Left*) in double-logarithmic representation known as the main sequence (22).

To test the detection algorithm against noise, we computed surrogate time series by constrained random-shuffling of the original velocity samples (23) for all trials of Exp. 1. We varied the detection threshold parameter λ of the algorithm and computed the average microsaccade rate over all trials as a function of λ (Fig. 1 *Lower Right*). Two main findings emphasize that our algorithm reliably identified microsaccades from fixational eye-movement trajectories. First, the algorithm detected more microsaccades in the original data than in the surrogate data over a broad range of threshold values ($\lambda = 3$ to $\lambda = 15$). Second, the difference between the rates obtained for original data and surrogates exhibits a maximum between $\lambda = 5$ and 7, which represents a maximum in the signal-to-noise ratio for the

Conflict of interest statement: No conflicts declared.

This paper was submitted directly (Track II) to the PNAS office.

Abbreviations: Exp. *n*, experiment *n*; IMSI, intermicrosaccade interval.

*To whom correspondence should be addressed. E-mail: engbert@uni-potsdam.de.

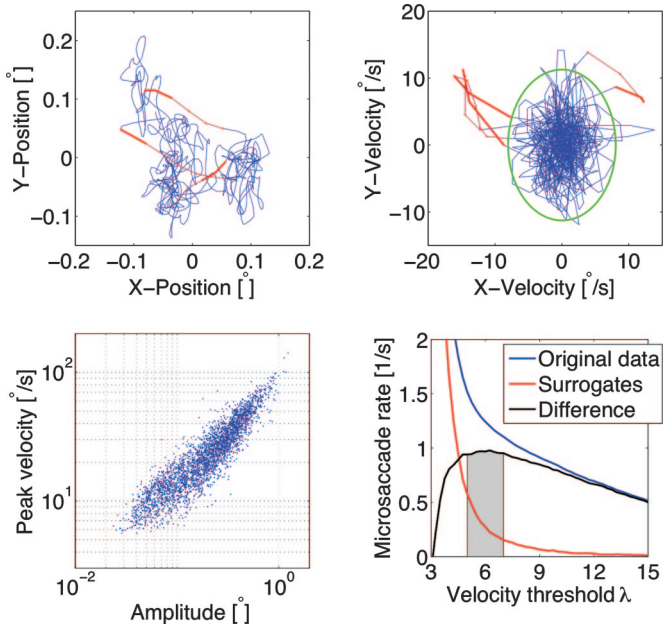

Fig. 1. Fixational eye movements and microsaccades. (*Upper Left*) Miniature eye movements recorded in Exp. 1 during a fixation of 3 s. Microsaccades are indicated by red color, where the last three data samples are highlighted by the bold line. (*Upper Right*) Same trajectory plotted in 2D velocity space. Independent detection thresholds for horizontal and vertical components (5 SDs) constitute an elliptic threshold criterion in 2D (green line). (*Lower Left*) Peak velocity and microsaccade amplitude are highly correlated, i.e., microsaccades follow the ''main sequence.'' (*Lower Right*) Average microsaccade rate computed from all trials of Exp. 1 by our algorithm as a function of the detection threshold λ (blue line). A lower average microsaccade rate is computed for surrogate data (red line), where the optimal signal-to-noise ratio is represented by the maximum of the difference of the two rates (black line).

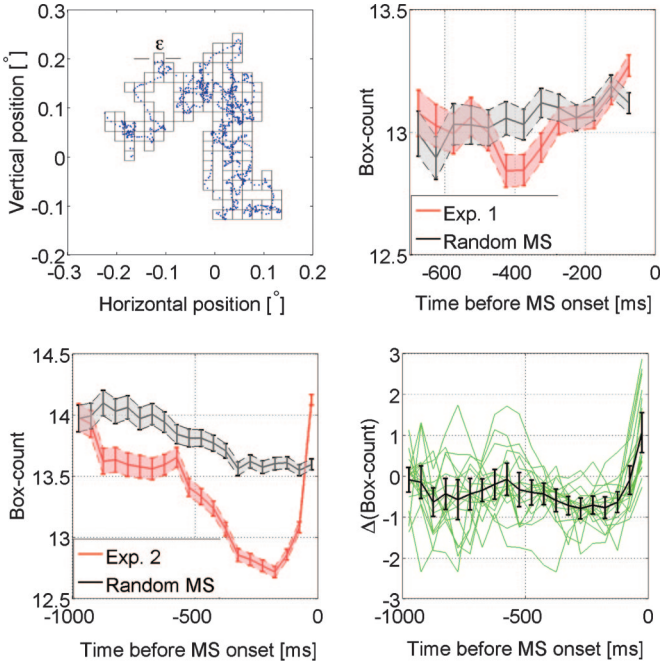

Fig. 3. Box-counting procedure and retinal image slip before microsaccades. (*Upper Left*) In the box-counting procedure, the number N_b of boxes with a linear dimension $\varepsilon = 0.01°$ needed to cover the graph of the trajectory is calculated as a measure of local retinal image slip. (*Upper Right*) In Exp. 1, the local box count N_b in time windows of 50 ms at different lags relative to microsaccade onset shows a significant drop at ≈−400 to −300 ms. (*Lower Left*) In Exp. 2, the same analysis yielded a decreased box count over a broad range of lags with a minimum value ≈−200 ms before microsaccade onset. (*Lower Right*) Interindividual differences in the box-count analysis. Box-count measures from the analysis with randomized saccade-onset times were subtracted from the box-count measures for original data (green curves represent results for individual participants). The negative mean values (black line with error bars representing standard errors) indicate a decreased box count before microsaccades for 15 of 17 participants and for a range of lags between −400 to −200 ms.

algorithm. We conclude that microsaccades can be distinguished from correlated noise by our algorithm. For further analyses reported here, we fix λ at a value of 5.

Distribution of Intermicrosaccade Intervals (IMSIs). The average microsaccade rate across participants was slightly >1 per second (1.13 s^{-1} in Exp. 1; 1.21 s^{-1} in Exp. 2). To compute intermicrosaccade intervals, only trials containing at least two microsaccades were considered. We observed more than one microsaccade in 897 of all 2,360 trials (or 38%) in Exp. 1, whereas we found more than one microsaccade in 375 of all 503 trials (or 75%) in Exp. 2. These trials were used to compute IMSIs (2,119 IMSIs in Exp. 1; 9,898 IMSIs in Exp. 2). In Exp. 1, a plot of the relative frequencies of IMSIs (Fig. 2 *Left*) indicates an exponential distribution (see Fig. 2 *Left Inset* with the same data plotted on a logarithmic vertical axis). An exponential distribution is compatible with the assumption of an underlying Poisson process (11) with constant probability over time for the occurrence of microsaccades. Thus, for the data obtained from Exp. 1, a probabilistic model of microsaccade generation seems adequate. In Exp. 2, the distribution of IMSIs again showed an exponential tail (see Fig. 2 *Right Inset*); however, there is a pronounced peak in the distribution of IMSIs at an interval duration of ≈500 ms. The observation of such a peak in the distribution of IMSIs, which indicates a periodic component of the generating process, can be interpreted as a first hint to an underlying dynamic mechanism of microsaccade triggering, which we will investigate by using a minimal stochastic model (see below).

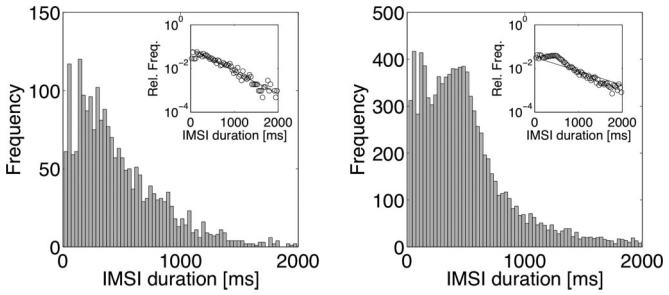

Fig. 2. Distributions of IMSIs. (*Left*) In Exp. 1, we observed an exponential distribution of IMSIs, which is demonstrated by the semilogarithmic plot given by *Inset*. (*Right*) In Exp. 2, IMSIs exhibited a more peaked distribution with a local maximum of ≈500 ms and an exponentially decaying tail.

Analysis of Retinal Image Slip. To characterize the amount of retinal image slip produced by fixational eye movements, we applied a box-counting approach, where the recorded eye trajectories were covered by boxes with a linear dimension of $\varepsilon = 0.01°$ (Fig. 3 *Upper Left*), corresponding to approximately the diameter of the cone receptive fields (24). We used the number of boxes N_b needed to cover the trajectory in a time window of 50 ms as a quantitative measure of retinal image slip. To investigate a possible correlation of this box-count measure with the later occurrence of microsaccades, we computed the value of N_b at different time lags before microsaccade onset, where the window of analysis was centered around the lag value (given on

the horizontal axis of Fig. 3 *Upper Right* and *Lower Left*). In Exp. 1, we find a decrease of the box-count measure ≈−400 ms to −300 ms before microsaccade onset (Fig. 3 *Upper Right*, red lines with bars representing standard errors). In Exp. 2, the decrease covers a broad range of lag between −500 ms and −100 ms before microsaccade onset (Fig. 3 *Lower Left*, red lines) showing a minimum value ≈−200 ms before microsaccade onset. The results indicate that low retinal image slip is correlated with the occurrence of microsaccades as a precursory phenomenon.

Our previous finding that a sudden display change induces a strong modulation of the microsaccades rate (20), which typically causes a transient over several seconds, could explain the weaker effects observed in Exp. 1, where the total fixation duration is only approximately one-seventh of the duration used in Exp. 2. Note also that there is an increased box count just before microsaccade onset, which is caused by a temporal jitter of the microsaccade onset times due to noise in the detection algorithm. The box-count estimation was based on epochs, which did not contain microsaccades to rule out any influence from previous microsaccades (consequently, the standard error increases with the delay due to a decreasing number of epochs available for the analysis).

To test the observed effect of decreased box count before microsaccades statistically, Monte Carlo simulations with randomly distributed microsaccade onset times were performed, which provided an estimate for fluctuations in the baseline of the box-count measure (Fig. 3 *Upper Right* and *Lower Left*, black lines). The box count N_b is significantly lower for the original data than for the random shuffled data (left-tailed t test; Exp. 1, $P < 0.005$ for a time lag of 400 ± 25 ms; Exp. 2, $P < 0.001$ for the same lag values). For Exp. 2, we carried out an analysis of interindividual differences, where the results for the difference between box count in original data and the value obtained from randomized saccade onset times were compared for participants (Fig. 3 *Lower Right*). Here, the values of the difference were negative (indicating decreased retinal image slip) for 15 from 17 participants (or 88%) at lag values between −200 and −400 ms. In a repeated-measures ANOVA with original data and randomized saccades as within-subject factor at a lag of −325 ms (within a centered window of 100 ms), differences were highly significant [$F(1, 16) = 39.5$; $P < 0.001$]. Because microsaccades are correlated with low values of N_b, insufficient retinal image slip might trigger the preparation of a microsaccade, which is executed with a rather broad latency distribution between −500 and −200 ms.

The estimate of the average latency for microsaccades is in agreement with saccadic reaction times to suddenly appearing stimuli. Activation in the superior colliculus is evoked by visual stimuli after 40 ms (25), whereas electrical stimulation of the superior colliculus generates a saccade after only 20 ms (26). Thus, saccadic responses with typical latencies ≈200 ms are not restricted by the physiological transmissions delays (60 ms). Instead, sensory accumulation processes (27–29) are responsible for the observed long latencies.

A Dynamical Model of Microsaccade Triggering. A minimal model for the generation of microsaccades can be built around the assumption that the estimation of retinal image slip is based on a sensory accumulator process. Because all sensory processes operate on noisy environmental signals, realistic models are inherently stochastic (30). For simplicity, we used a long realization (n = 300,000 data points) of a random walk with uncorrelated Gaussian-distributed velocity samples (Fig. 4 *Left* shows a representative epoch of 900 data points of the simulated trajectory).

The model was implemented in three steps. First, the same box-counting procedure was applied to the simulated data as was applied to the original data (see Fig. 3 *Upper Left*). Second, we assumed that evidence for low retinal slip accumulates over time, where a counter is incremented by one whenever the box count is smaller than the average box count decreased by 2 SDs. For all other cases, the counter value is kept constant. Thus, the accumulator process yields a monotonically increasing counter value as illustrated in Fig. 4 *Right* for the first 1,500 data points of the simulated random walk. Third, we implemented the rule that a microsaccade is triggered (indicated by the arrows in Fig. 4 *Right*) whenever a counter value of δ is reached (in Fig. 4 *Right*, we applied δ = 25).

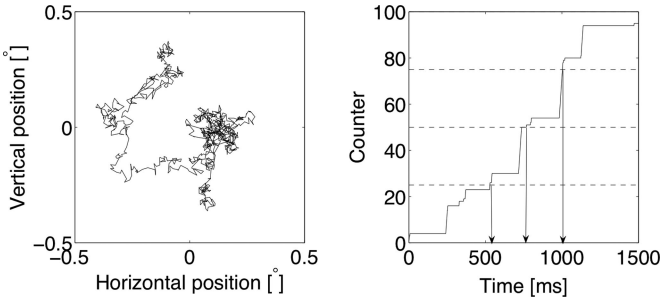

Fig. 4. A sensory accumulator model of microsaccade generation. (*Left*) A segment of 900 data points from simulated random walk used for the analysis (see *Methods*). (*Right*) The temporal evolution of the counter value in the accumulator model. In the illustration, a microsaccade is triggered whenever the counter passes the threshold after a distance of δ = 25 counts (indicated by arrows).

For a low value of δ, we obtained an exponential distribution of IMSIs (Fig. 5 *Left* with δ = 10), whereas for a high value of δ, the distribution of IMSIs shows a clear peak (Fig. 5 *Right* with δ = 20). Thus, our minimal model can reproduce the qualitative features of the distributions of IMSIs obtained from Exp.1 and Exp. 2. We conclude that a dynamical mechanism for triggering of microsaccades is in good agreement with experimental data.

Fractal Dimension Analysis. The observed interindividual variability of microsaccade rate between participants poses a problem for any potential mechanism of the generation of microsaccades. In Exp. 1, the microsaccade rate varied between a minimum of 0.31 s^{-1} and a maximum of 2.04 s^{-1} (mean value: 1.13 s^{-1}). Similar values were obtained from Exp. 2, where microsaccade rate was distributed over a range from 0.19 s^{-1} to 2.72 s^{-1} (mean value: 1.21 s^{-1}). If microsaccades are crucial for the generation of sufficient retinal image slip, why do we observe such a broad range of microsaccade rates across participants? Based on the above mechanism of dynamic triggering of microsaccades, the source of this variation is likely to be found in a related variation of the slow movement components (drift and tremor). Using the

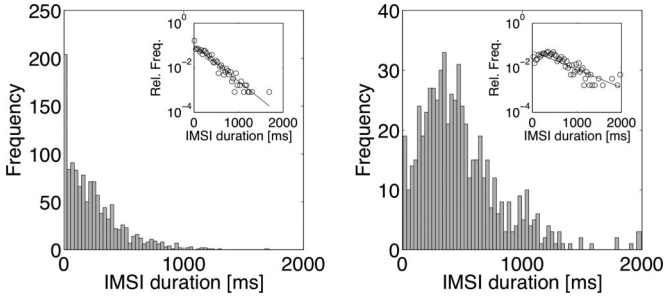

Fig. 5. Distributions of IMSIs obtained from model simulations. (*Left*) For δ = 10, the model generates exponentially distributed IMSIs, which is qualitatively in good agreement with results from Exp. 1. (*Right*) For δ = 20, the distribution of IMSIs shows a pronounced peak similar to the results from Exp. 2.

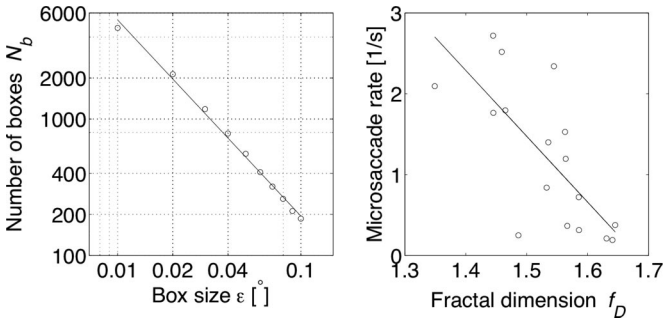

Fig. 6. Fractal dimension and microsaccade rate. (*Left*) To characterize the geometry of the trajectories, we computed the number of boxes N_b as a function of the linear dimension ε. The fractal dimension can be read off from the exponent of the resulting power law. (*Right*) The average fractal dimension (computed from all trials of a participant) is negatively correlated with the average microsaccade rate. Each data point represents data from one participant. The fractal dimension was computed for the drift component of fixational eye movements, i.e., after removing all microsaccades.

box-counting approach, we noticed that variation of the length scale ε yields a power law for the box count N_b as a function of ε, $N_b(\varepsilon) \propto \varepsilon^{-f_D}$, indicating statistical self-similarity (31), where f_D is the fractal (or box-counting) dimension of the trajectory (Fig. 6 *Left*). To exclude possible influences from microsaccades, we removed microsaccades from the trajectories (see *Methods*) and calculated the average fractal dimension of trajectories from all trials of a participant. The higher the fractal dimension of the trajectory, the more space filling is the resulting curve. When plotting the average fractal dimension f_D against microsaccade rate m for all participants of Exp. 2 (Fig. 6 *Right*), we observed a significant negative correlation with the rate of microsaccades ($r = -0.72$; $P < 0.005$). In Exp. 1, we also obtained a significant negative correlation ($r = -0.40$; $P < 0.05$); however, the results from Exp. 2 are probably more reliable because of the longer time series. Because a high fractal dimension is related to a low microsaccade rate, microsaccades occur more frequently when the area covered by the slow movements is small. Therefore, the correlation might be caused by the dynamic mechanism postulated above.

Discussion

Our study was motivated by two different possible mechanisms for the generation of microsaccades: First, the generation of microsaccades might represent a purely stochastic process with constant probability over time (i.e., a Poisson process with exponentially distributed IMSIs). Second, microsaccades might be generated dynamically in response to low retinal image slip to counteract retinal fatigue. Using a box-counting procedure, we found support for the latter hypothesis in data from two experiments. Before microsaccade onset times, retinal image slip was significantly decreased compared with randomly chosen epochs of the trajectories. The observed latency between low retinal image slip and microsaccade onset ranged roughly between 200 and 500 ms. Thus, typical saccadic reaction times provide a lower bound for the generating process, which is compatible with a dynamical triggering mechanism based on a sensory accumulator model. We implemented a minimal computational model of such an accumulator model to demonstrate that a dynamical triggering mechanism can account for the experimentally observed distributions of IMSIs. We expect that there are additional processes modulating the rate of microsaccades, of course, but because our model basically controls microsaccade rate, such additional processes may coexist with the principles implemented in our model.

If microsaccades are triggered dynamically in response to statistical properties of retinal image slip produced by the drift component of fixational eye movements, then the empirically observed variation in microsaccade rate across participants should be caused by interindividual variations of the statistical properties of the drift. After removing microsaccades from the trajectories, we carried out an analysis of the fractal dimension of the resulting drift trajectory. The higher the fractal dimension value is, the more space filling is the resulting trajectory. Therefore, we expected a lower microsaccade rate for participants showing a higher fractal dimension. We obtained the hypothesized negative correlation between microsaccade rate and fractal dimension, supporting our hypothesis that drift epochs with low fractal dimension did not provide sufficient retinal image slip. As a consequence, participants with a low fractal dimension of the drift component of fixational eye movements generated a high microsaccade rate.

An interesting problem for further research is related to the exact mechanisms of microsaccade triggering. The simplest dynamical principle is based on monitoring the oculomotor system itself. In this case, our box-count measure would be very close to the physiological mechanism. An alternative mechanism is, however, based on the perceptual needs, so that a loop involving the visual stream would be an important component of the control circuitry for the generation of microsaccades.

Using statistical analyses of the eye's random walk, we previously have uncovered a time scale separation between error-production and error-correction of microsaccades (8): On a short time scale (<20 ms), microsaccades enhance retinal image slip by inducing persistent correlations, so that the eye maintains its current movement direction, whereas on a longer time scale (>40 ms), microsaccades help to prevent the loss of current fixation position by reversing current movement direction due to antipersistent correlations. These findings suggest that both large fixation errors or small retinal image motion are candidate mechanisms for triggering microsaccades if microsaccades do not follow simple Poisson statistics. The current results suggest that insufficient retinal image slip is one signal for the generation of microsaccades.

Recently, it was observed that microsaccades can induce transitions from fading to intensifying percepts of peripheral stimuli during Troxler fading (19). This important finding represents a direct link between oculomotor behavior and visual perception. Given such a critical function of microsaccades for perception, a dynamical triggering of microsaccades seems highly plausible.

More generally, new findings in different domains of research emphasize the relevance of microsaccades to oculomotor control, visual perception, and attention. First, it has been found that microsaccades modulate neural activity in several areas along the visual stream, including excitatory-bursting activity in macaque area V1 (32) and also in the LGN (33). Second, microsaccades are modulated by visual attention and might provide a tool to map the time course of visual attention in attentional cuing paradigms (refs. 20 and 34–36; for an overview, see ref. 37).

Taken together with the recent finding that microsaccades enhance the perception of peripheral stimuli (19), our results demonstrate that vision is critically based on motor behavior, in contrast to the dominant view that human movements are based on visual perception. Finally, we expect that our approach to the investigation of fixational eye movements and microsaccades proposed here will be an interesting tool for the analysis of data obtained from more dynamic task like reading (38) or visual search (39).

Methods

Participants and Task. Participants were required to fixate a small stimulus (black square on white background, 3 × 3 pixels on a computer display) with spatial extent of 0.12° (or 7.2 arc min). All participants were instructed to keep their eyes on the fixation spot and to prevent eye blinks. Participants received a payment of 5 euros.

Experiment 1. We asked 29 participants to perform 100 trials with a duration of 3 s.

Experiment 2. Within the same fixation paradigm, 17 participants (students of the University of Potsdam) were asked to perform 30 trials with a trial duration of 20 s. Because of the long fixation duration, the prevention of massive loss of trials due to blinks was critical. We implemented an automatic screening for missing data samples during the experiment. If missing samples were detected, trials were immediately aborted and then restarted. Participants were informed on this procedure in advance and that eye blinks should be prevented. Because of the unnaturally long fixations, we presented photographs (10 s each) between trials to give participants the possibility to produce inspection saccades and eye blinks.

Eye-Movement Recording and Data Preprocessing. Eye movements were recorded by using an EyeLink-II system (SR Research, Osgoode, ON, Canada) with a sampling rate of 500 Hz and an instrument spatial resolution of 0.01°. Participants' head movements were minimized by using a chin rest (and an additional biteboard in Exp.1). Raw data were smoothed by using a running average on velocity samples to suppress high-frequency noise. Velocities were computed from raw data samples $\vec{x}_n$ according to a moving average procedure (20),

$$\vec{v}_n = \frac{\vec{x}_{n+2} + \vec{x}_{n+1} - \vec{x}_{n-1} - \vec{x}_{n-2}}{6\Delta t}, \qquad [1]$$

where $\Delta t = 500$ ms is the sampling interval. To suppress noise, position values were reconstructed by performing a cumulative sum, i.e.,

$$\vec{x}_n = \vec{x}_o + \Delta t \cdot \sum_{i=1}^{n} \vec{v}_n. \qquad [2]$$

Experiment 1. During preprocessing, 540 of 2,900 trials (or 19%) were discarded because of missing data samples due to eye blinks or saccades with amplitudes >1°.

Experiment 2. Missing data samples due to eye blinks were detected during the experiment. Therefore, during preprocessing, only 7 of 510 trials (or 1.4%) were discarded, because they contained saccades with amplitudes >1°.

Microsaccade Detection. Microsaccades were detected in 2D velocity space by using thresholds for peak velocity and a minimum duration, implemented as an improved version of an algorithm proposed earlier (20). We used relative thresholds, separately computed for horizontal (η_x) and vertical (η_y) components in units of median-based SDs, $\eta_{x,y} = \lambda \cdot \sigma_{x,y}$, where $\sigma^2_{x,y} = \langle (v_{x,y} - \langle v_{x,y} \rangle)^2 \rangle$. Thus, an elliptic threshold in 2D velocity space resulted (Fig. 1 *Upper Right* for $\lambda = 5$). Additionally, a minimal duration of three data samples (or 6 ms) was applied; i.e., a microsaccade was detected only if three or more data samples were outside the ellipse defined by the horizontal and vertical threshold. Finally, we considered only binocular microsaccades, which we defined as microsaccades detected in both eyes with a temporal overlap of at least one data sample. For clusters consisting of microsaccades with multiple overlapping relations, we selected the largest microsaccades from both eyes within the cluster.

Testing the Algorithm Against Noise. The reliability of the procedures for microsaccade detection were evaluated by numerical simulations by using phase-randomized amplitude-adjusted surrogate data (23). For each trial from Exp. 1, we computed the corresponding time series of velocities (see above). For velocity series, surrogate data were obtained by constrained random shuffling of the original time series (i.e., randomization of the phase of the Fourier spectrum and remapping onto the original velocity samples). Therefore, the distribution of velocity values was exactly the same as in the original data, and the autocorrelation function of the original velocity series was approximated by the surrogate data. The performance of the algorithm showed that more microsaccades were detected in the original data than in the surrogate data over a broad range of detection threshold parameter values λ (Fig. 1 *Lower Right*).

Removing Microsaccades. To remove microsaccades from the experimentally observed trajectories, first, we computed the increments of the trajectory, second, we removed all increments corresponding to microsaccades, and, third, we reconstructed the trajectory by performing a cumulative sum (9).

Model Simulations. Velocities were implemented as uncorrelated Gaussian-distributed random variables with statistically independent horizontal (v_x) and vertical components (v_y) and a standard deviation of 0.015°/s. A sample trajectory of n = 300,000 data points was generated for the box-counting analysis (Fig. 4 *Left*, showing a segment of 900 data points of the trajectory). According to the model, low retinal image slip is detected by an accumulator process. First, we computed the box count ($\varepsilon = 0.01°$) by using a running average of 25 data points. Second, whenever the box count dropped to values <2 SDs below the average box count, the counter of the accumulator process was increased by one unit (otherwise the counter value remained unchanged). The resulting counter time series of the accumulator process is shown in Fig. 4 *Right*. Third, microsaccade were triggered, when a threshold of δ steps were reached in the counter (in Fig. 4 *Right* we used $\delta = 25$). For a value of $\delta = 10$, we obtain an exponential distribution of IMSIs, whereas there is a pronounced peak in the distribution of for higher values of the threshold δ.

We thank Petra Grüttner for research assistance (Exp. 1) and Reinhold Kliegl, Susana Martinez-Conde, and an anonymous reviewer for valuable comments on the manuscript. This work was supported by Deutsche Forschungsgemeinschaft Grant KL 955-3/3.

1. Ditchburn, R. W. & Ginsborg, B. L. (1952) *Nature* **170,** 36–37.
2. Riggs, L. A., Ratliff, F., Cornsweet, J. C. & Cornsweet, T. N. (1953) *J. Opt. Soc. Am.* **43,** 495–501.
3. Ratliff, F. & Riggs, L. A. (1950) *J. Exp. Psychol.* **40,** 687–701.
4. Wade, N. J. & Tatler, B. W. (2005) *The Moving Tablet of the Eye* (Oxford Univ. Press, Oxford).
5. Carpenter, R. H. S. (1988) *Movements of the Eyes* (Pion, London).
6. Yarbus, A. L. (1967) *Eye Movements and Vision* (Plenum, New York).
7. Martinez-Conde, S., Macknik, S. L., & Hubel, D. H. (2004) *Nat. Rev. Neurosci.* **5,** 229–240.
8. Engbert, R. & Kliegl, R. (2004) *Psychol. Sci.* **15,** 413–435.
9. Klafter, J., Shlesinger, M. F. & Zumofen, G. (1996) *Phys. Today* **49,** 33–39.
10. Shlesinger, M. F. (2001) *Nature* **411,** 641.
11. Cox, D. R. & Miller, H. D. (1965) *The Theory of Stochastic Processes* (Methuen, London).
12. Engbert, R. (2006) *Neuron* **49,** 168–170.
13. Nachmias, J. (1959) *J. Opt. Soc. Am.* **49,** 901–908.
14. Cornsweet, T. N. (1956) *J. Opt. Soc. Am.* **46,** 987–993.
15. Winterson, B. J. & Collewijn, H. (1976) *Vision Res.* **16,** 1387–1390.
16. Bridgeman, B. & Palca, J. (1980) *Vision Res.* **20,** 813–817.
17. Steinman, R. M., Cunitz, R. J., Timberlake, G. T. & Herman, M. (1967) *Science* **155,** 1577–1579.

18. Kowler, E. & Steinman, R. M. (1980) *Vision Res.* **20,** 273–276.
19. Martinez-Conde, S., Macknik, S. L., Troncoso, X. G. & Dyar, T. A. (2006) *Neuron* **49,** 297–305.
20. Engbert, R. & Kliegl, R. (2003) *Vision Res.* **43,** 1035–1045.
21. Zuber, B. L., Stark, L. & Cook, G. (1965) *Science* **150,** 1459–1460.
22. Bahill, A. T., Adler, D. & Stark, L. (1975) *Math. Biosci.* **24,** 191–204.
23. Theiler, J., Eubank, S., Longtin, A., Galdrikian, B. & Farmer, J. D. (1992) *Physica D* **58,** 77–94.
24. Ölveczky, B. P., Baccus, S. A. & Meister, M. (2003) *Nature* **423,** 401–408.
25. Guitton, D. (1992) in *Eye Movements*, ed. Carpenter, R. H. S. (McMillan, London), pp. 244–276.
26. Sparks, D. L. (1986) *Physiol. Rev.* **66,** 118–171.
27. Carpenter, R. H. S. & Williams, M. L. L. (1995) *Nature* **377,** 59–62.
28. Reddi, B. A. J. & Carpenter, R. H. S. (2001) *Nat. Neurosci.* **3,** 827–830.
29. Ratcliff, R. (2001) *Nat. Neurosci.* **4,** 336.
30. Ratcliff, R. (1978) *Psychol. Rev.* **85,** 59–108.
31. Mandelbrot, B. B. (1967) *Science* **155,** 636–638.
32. Martinez-Conde, S., Macknik, S. L. & Hubel, D. H. (2000) *Nat. Neurosci.* **3,** 251–258.
33. Martinez-Conde, S., Macknik, S. L. & Hubel, D. H. (2002) *Proc. Natl. Acad. Sci. USA* **99,** 13920–13925.
34. Hafed, Z. M. & Clark, J. J. (2002) *Vision Res.* **42,** 2533–2545.
35. Laubrock, J., Engbert, R. & Kliegl, R. (2005) *Vision Res.* **45,** 721–730.
36. Rolfs, M., Engbert, R. & Kliegl, R. (2005) *Exp. Brain Res.* **166,** 427–439.
37. Engbert, R. (2006) *Prog. Brain Res.*, in press.
38. Engbert, R., Nuthmann, A., Richter, E. & Kliegl, R. (2005) *Psychol. Rev.* **112,** 777–813.
39. Gilchrist, I. D. & Harvey, M. (2000) *Curr. Biol.* **10,** 1209–1212.